ELSEVIER

Journal of Alloys and Compounds 293–295 (1999) 556–563

Journal of ALLOYS AND COMPOUNDS

Electrochemical characteristics of nanocrystalline $ZrCr_2$ and Mg_2Ni type metal hydrides prepared by mechanical alloying

Jung Hoon Woo, Chang Bo Jung, Jung Hoon Lee, Kyung Sub Lee*

Department of Metallurgical Engineering, Hanyang University, Seoul 133-791, South Korea

Abstract

The mechanical alloying process (MA) has been introduced to produce nanocrystalline $ZrCr_2$ and Mg_2Ni type metal hydride. MA has recently emerged as a novel technique for producing alloy powders whose structures are nanocrystalline. The Zr–Cr–Ni and Mg–Ni systems were prepared using a planetary ball mill, starting from mixtures of elemental powders. In the Zr–Cr–Ni system, nanocrystalline C14 structure could not be obtained after ball-milling but could be obtained from heat-treatment of ball-milled powders. The heat-treated Zr–Cr–Ni powders showed a similar discharge capacity to the arc-melted alloy, but the activation was much easier. In contrast to Zr–Cr–Ni system, nanocrystalline Mg_2Ni alloy could be formed by ball-milling. In comparison with the polycrystalline one, nanocrystalline Mg_2Ni showed a lower temperature for hydrogenation and a much higher discharge capacity at 30°C. The partial substitution of Zr for Mg resulted in a microstructure different from mechanically alloyed Mg_2Ni and greatly improved the discharge capacity at 30°C. The discharge capacity of 120 h-milled 1.8Mg–0.2Zr–Ni electrode was 465 mAh g^{-1}.

Keywords: $ZrCr_2$ and Mg_2Ni type alloy; Mechanical alloying; Heat-treatment; Nanocrystalline; Hydrogenation

1. Introduction

A number of studies have been carried out extensively on the AB (TiFe), AB_2 ($ZrCr_2$, $TiCr_2$), AB_5 ($LaNi_5$) and A_2B (Mg_2Ni) type hydrogen storage alloys which have been developed as the anodic materials of Ni/MH batteries [1,2]. Among these types, Zr-based Laves phase alloys are attractive due to their higher discharge capacities but they have a disadvantage of requiring many charge–discharge cycles for activation [3]. Mg_2Ni type alloys are promising materials because of their high hydrogen storage capacity (up to 3.6 wt%), low material cost and rich mineral sources [4,5]. However, they can absorb and desorb hydrogen at high temperature (above 300°C) and the discharge capacity is very low at low temperature (below 30°C) [6]. Moreover, it is very difficult to synthesize Mg_2Ni type alloys by conventional melting processes due to their large differences in melting temperature.

In this study, a mechanical alloying process has been introduced to produce AB_2 ($ZrCr_2$) and A_2B (Mg_2Ni) type metal hydride. Mechanical alloying is a dry, high energy ball milling process, which has been used to prepare several dispersion strengthened alloy powders [7,8]. More recently, this process has been adopted to synthesize intermetallics and other inorganic nonmetallics. When the mechanical alloying process by the ball milling technique is used for such synthesis, the powders show unusual characteristics such as nanocrystalline structures [9], amorphous materials [10,11] and alloys with extended solubilities [12]. Moreover, some interest has developed in nanocrystalline alloys since their hydriding properties are different from those of conventional crystalline ones [13–16].

In the present study, Zr–Cr–Ni and Mg–Ni systems were prepared by the planetary ball mill, starting from the elemental powders. The synthesized nanocrystalline alloys were expected to improve the hydrogenation and electrochemical characteristics of the metal hydride electrode. In order to improve the electrode characteristics of mechanically alloyed Mg_2Ni, partial substitution of Zr for Mg was carried out.

2. Experimental

The starting materials for the ball milling were the mixtures of the elemental powders. To prepare the starting materials from elemental powders, the elemental powders

*Corresponding author.

0925-8388/99/$ – see front matter
PII: S0925-8388(99)00411-9

with a particle size of less than 46 μm and purity 99.9% were mixed to give the desired composition. The particle size of Mg was less than 175 μm. The specific compositions made for this report were: Zr–Cr–Ni, 2Mg–Ni and 1.8Mg–0.2Zr–Ni. These starting materials were put into a CrNi-steel bowl together with stainless steel balls (SUS304, 2/16 inch in diameter). The handling of the powders was done in an argon-filled glove box in order to prevent oxidation of powders. Mechanical alloying was carried out using a planetary ball mill (Fritsch Pulverisette 5) at a speed of 300 rpm for the Zr–Cr–Ni system and 100 rpm for the Mg–Ni system. Milling speed could not exceed 100 rpm for the Mg–Ni system because ductile Mg and Ni were cold-welded to ball and bowl.

The structures of the ball-milled powders were characterized by X-ray diffraction (XRD) analysis using CuKα radiation (λ=1.5418 Å). Microstructure studies were performed by SEM and TEM. In order to determine the heat-treatment condition, differential thermal analysis (DTA) was carried out. Heating was performed at a rate of 5 K min^{-1} in a pure argon flow.

The alloy powders were mixed with electrolytic Ni powder in a weight ratio of 1:2 and mechanically pressed into a pellet of 1.0 cm in diameter under a pressure of 5 ton cm^{-2} to prepare working electrodes. The negative electrode had an active material of about 0.1 g. The electrochemical measurements were conducted in a half cell which consisted of metal hydride as a working electrode, a platinum counter electrode and a Hg/HgO reference electrode in 6 M KOH electrolyte. Cycle tests were performed at 30°C using an automatic galvanostatic charge–discharge unit (Maccor series 4000) at a constant current of 10 mA g^{-1}. The discharge cut-off potential was set to −0.60 V with respect to the reference electrode. The resting time between charge and discharge was 5 min. Pressure–composition (P–C) isotherms were measured at various temperature by a conventional Sievert's type apparatus. About 1 g of powder was put into the stainless steel reactor.

3. Results and discussion

3.1. Zr–Cr–Ni system

3.1.1. Microstructure analysis

Fig. 1 shows the XRD patterns of the Zr–Cr–Ni system: (a) the 30 h ball-milled powders and (b) heat-treated powders after 30 h ball-milling. In the 30 h-milled Zr–Cr–Ni powders, the elemental peaks were visible even though their intensities decreased. Moreover, instead of the formation of the $ZrCr_2$ type compound, other phases (such as Ni_7Zr_2, $Ni_{11}Zr_9$ and ZrO_2) appeared. HREM observation was performed in order to further characterize the microstructure of the 30 h-milled Zr–Cr–Ni powder. As shown in Fig. 2, the nanocrystalline atomic arrays (such as Zr, Ni_7Zr_2, $Ni_{11}Zr_9$, and ZrO_2) with different orientations were observed and some areas showed an amorphous-like structure. However, no evidence of $ZrCr_2$ type Laves phase could be also found in the HREM observation. Further milling did not result in the formation of hydrogen storage $ZrCr_2$ type alloy. In this study, the XRD pattern

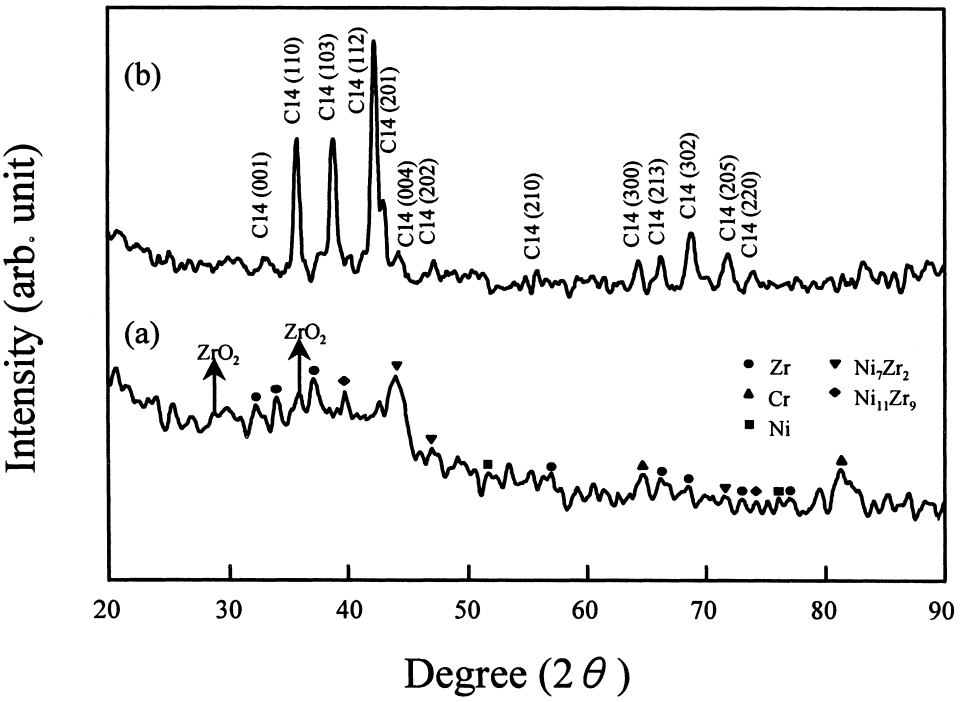

Fig. 1. X-ray diffraction patterns of the 30 h-milled and the heat-treated Zr–Cr–Ni powders: (a) 30 h ball-milled; (b) heat-treated (900°C, 3 h).

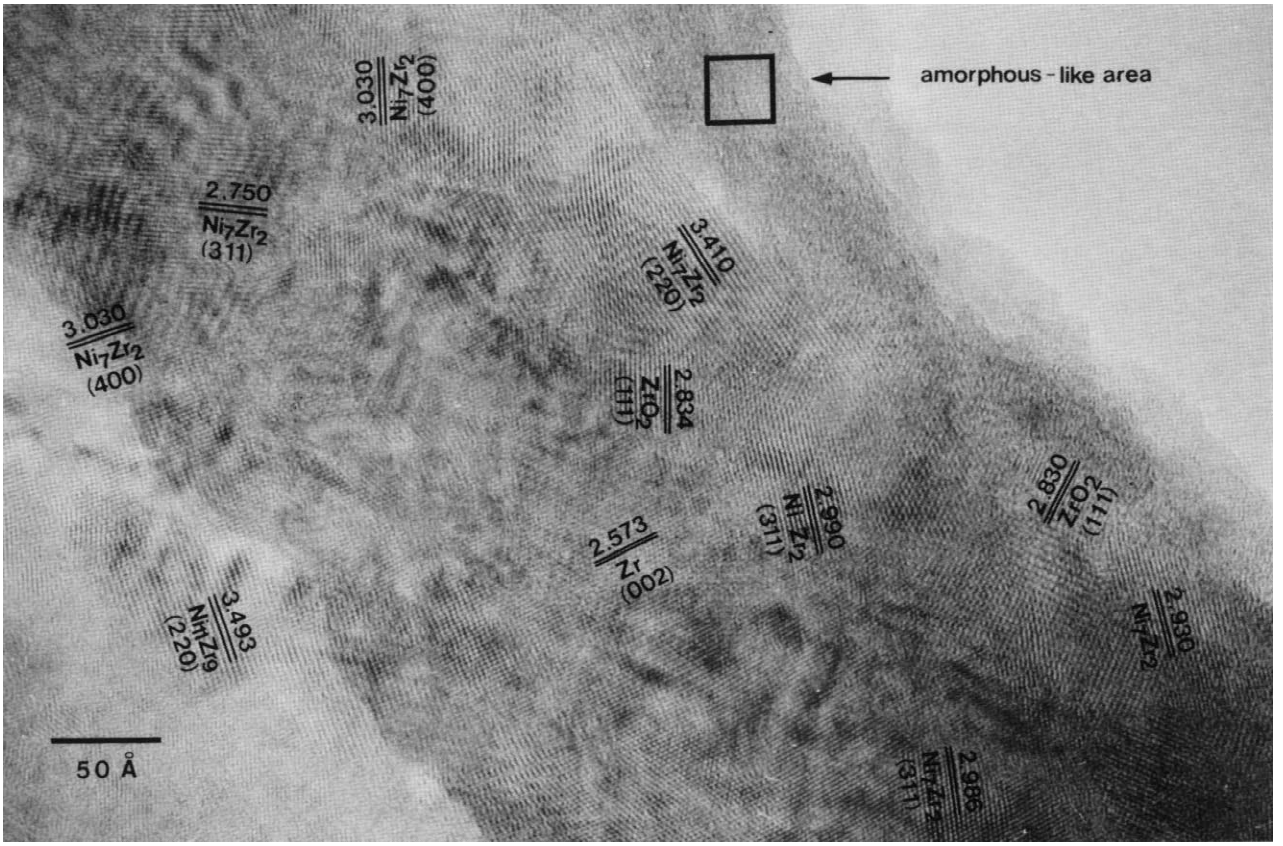

Fig. 2. HREM micrographs of the 30 h-milled Zr–Cr–Ni powder.

and HREM results were in good agreement with the work of the Hellstern and Schultz [10,11]. They reported that the V–Zr and the Cr–Zr system can not be mechanically alloyed due to low heat of mixing but consist of a microscopic mixture of the starting elements after milling. To study the chemical driving force for the ball milling, Hellstern and Schultz calculated the heat of mixing within the TM (transition metal)–Zr system using the semiempirical approach of Niessen et al. [17]. Their results showed that the Ni–Zr had a large negative free enthalpy of mixing but the Cr–Zr possessed the lowest mixing tendency in the TM–Zr series. In this study, therefore, it seems likely that some Ni–Zr compounds (such as Ni_7Zr_2, $Ni_{11}Zr_9$) are formed, but mostly the ball-milled Zr–Cr–Ni powder consists of a microscopic mixture of the starting elements.

In order to synthesize nanocrystalline $Zr(Cr_{0.5}Ni_{0.5})_2$ alloy of C14 structure, 30 h-milled Zr–Cr–Ni powders were heat-treated. The phase transformation behavior of 30 h-milled Zr–Cr–Ni powders during heat-treatment was examined by DTA. As shown in Fig. 3, the DTA curve consists of two exothermic peaks and one endothermic peak. The first (554°C) and second (850°C) exothermic reactions are probably the release of the stored energy introduced by mechanical deformation and the formation of $ZrCr_2$ type Laves phase, respectively. The last endothermic peak (1351°C) implies the melting of the powder by the eutectic reaction of Zr–Cr according to the equilibrium diagram of Zr–Cr [18].

To confirm the crystallization of 30 h-milled Zr–Cr–Ni powder, by heat-treatment, XRD, HREM observation were carried out. The ball-milled powder was heat-treated for 3 h at 900°C under vacuum ($5 \cdot 10^{-6}$ Torr). As shown in Fig. 1b, the XRD pattern was of the C14 type Laves phase after heat-treatment. The electron diffraction pattern of the heat-treated powder was also of the C14 Laves phase and the microstructure consisted of small grains less than 100 nm (Fig. 4). This result also suggests that a nanocrystalline alloy can be produced by means of heat-treatment after ball-milling.

3.1.2. P–C isotherms and electrochemical measurements

Fig. 5 shows the hydrogen desorption characteristics at 30°C for ball-milled Zr–Cr–Ni and heat-treated powders. For the 30 h-milled Zr–Cr–Ni powder, a very small amount of hydrogen was absorbed and desorbed. It is related to the microstructure of the ball-milled powder which consists of the microscopic mixture of the starting elements and has no hydrogen storage compounds. However, the *P–C* isotherm of heat-treated Zr–Cr–Ni powder showed that the hydrogen uptake equals about 1.3 wt% of hydrogen at 5 MPa and the reversible amount of desorbed hydrogen is about 0.9 wt% at the plateau pressure of 0.3

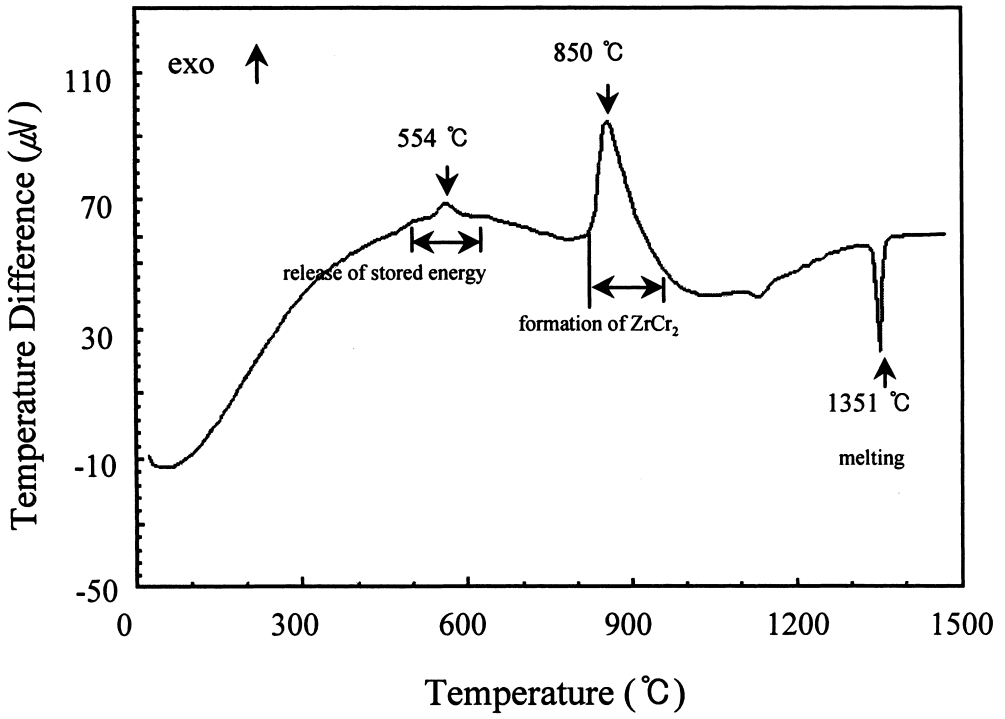

Fig. 3. DTA curve of the 30 h-milled Zr–Cr–Ni powders.

Mpa. This is probably due to the formation of the C14 type Laves phase after the heat-treatment.

Fig. 6 shows the variation of discharge capacity with cycle number. The discharge capacity of 30 h-milled Zr–Cr–Ni was very low because hydrogen storage material was not formed. However, the heat-treated Zr–Cr–Ni electrode showed a discharge capacity of 238 mAh g^{-1}, slightly lower than in the as-melted one which was reported by Jung et al. [19,20]. Additionally, the heat-treated electrode was activated after five charge–discharge cycles which is three times faster than that of as-melted electrode. Jung et al. [20] reported that the discharge capacity of as-melted $Zr(Cr_{0.5}Ni_{0.5})_2$ electrode reached a maximum value (257 mAh g^{-1}) after the 15th cycle. The improved activation characteristics seems to be related to the small grain size (≤100 nm) and the defects introduced by mechanical deformation. Also Zaluski and coworkers reported that the activation of nanocrystalline Fe–Ti was much easier [21,22].

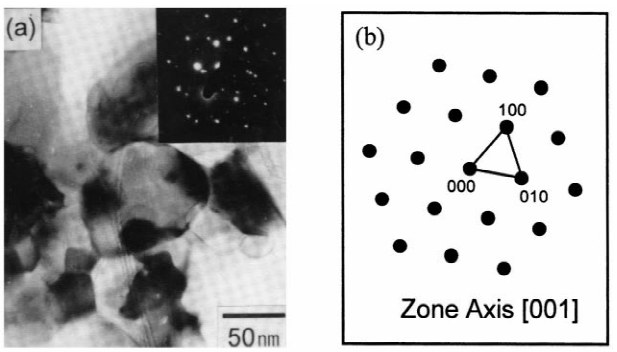

Fig. 4. HREM micrographs of the heat-treated Zr–Cr–Ni: (a) bright field; (b) electron diffraction pattern.

3.2. Mg–Ni system

3.2.1. Microstructure analysis

Fig. 7a shows the XRD pattern of 120 h-milled 2Mg–Ni powders. Although the trace of elemental Ni remained, Mg disappeared completely and transformed to Mg_2Ni phase. The trace of elemental Ni peaks did not disappear on further milling. The diffraction pattern of 120 h-milled powders exhibits broadening of peaks which is the characteristic of nanocrystalline material. The 120 h-milled powders were examined by TEM. Fig. 8 shows the bright-field image (a), dark-field image (b) and SAD pattern (c) of 120 h-milled 2Mg–Ni powders. It was found that a typical nanocrystalline particle (less than 20 nm) was produced by the mechanical alloying and the electron diffraction pattern shows that the phase in this area is Mg_2Ni. Similar observations have been reported by Singh et al. and Zaluski et al. [23,24].

Zr was partially substituted for Mg and the mixture of these elemental powders was ball-milled for 120 h. The XRD pattern of substituted alloy is shown in Fig. 7b. The pattern of 1.8Mg–0.2Zr–Ni shows broad peaks different from that of 120 h-milled 2Mg–Ni. The microsturcture of 120 h-milled 1.8Mg–0.2Zr–Ni seems to be amorphous structure. Fig. 9 shows the bright-field image (a) and SAD

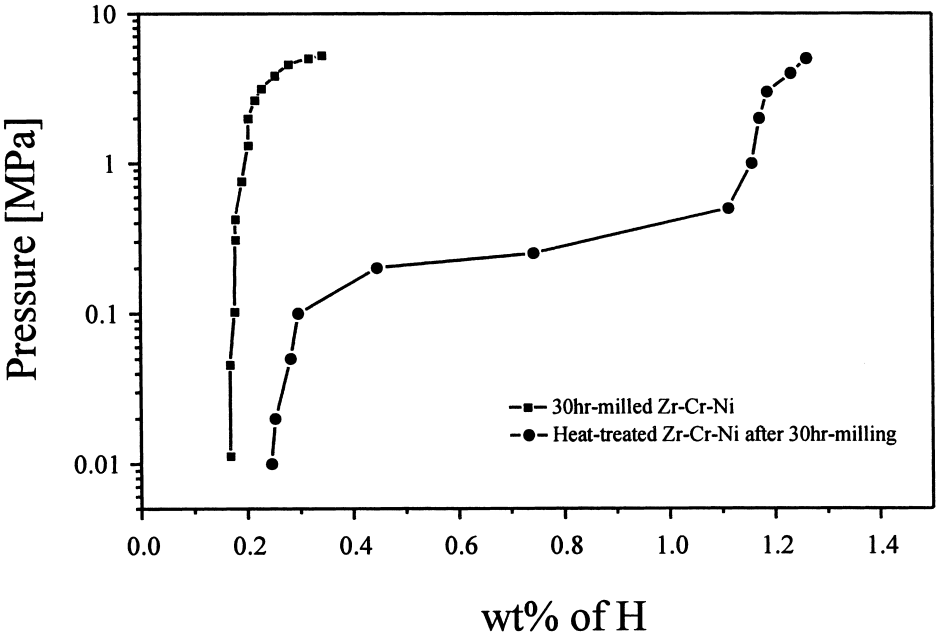

Fig. 5. Pressure–composition isotherms of 30 h-milled and heat-treated Zr–Cr–Ni powders measured at 30°C.

pattern (b) of 120 h-milled 1.8Mg–0.2Zr–Ni powders by TEM observation. It was found that amorphous matrix and nanostructured precipitate was produced by mechanical alloying. The precipitates were confirmed as Mg_2Ni phase in SAD pattern. The differences between 2Mg–Ni and 1.8Mg–0.2Zr–Ni observed in microstructure analysis were expected to result in different hydrogenation and electrochemical characteristics.

3.2.2. P–C isothermal measurements

Fig. 10 shows the hydrogen desorption characteristics at various temperature for the 120 h-milled 2Mg–Ni. The *P–C* isotherm at 300°C shows that the hydrogen uptake equals about 3.75 wt% of hydrogen at 5 Mpa and the reversible amount of desorbed hydrogen is about 3.2 wt% at the plateau pressure of 0.2 MPa. The result at 300°C is similar to that of the polycrystalline one which was reported by Reilly and Wiswall [4].

The *P–C* isotherm at 30°C shows that nanocrystalline Mg_2Ni powders absorbed 0.7 wt% of hydrogen and desorbed a small amount of hydrogen. It means that nanocrystalline Mg_2Ni does not improve the poor hydrogenation characteristics of conventional polycrystalline one at 30°C.

However, at 200°C, the amount of 2.8 wt% hydrogen was absorbed at 5 MPa and the reversible amount of about 1.5 wt% hydrogen was desorbed at the plateau pressure of $8.0 \cdot 10^{-3}$ MPa. The result at 200°C means that nanocrystal-

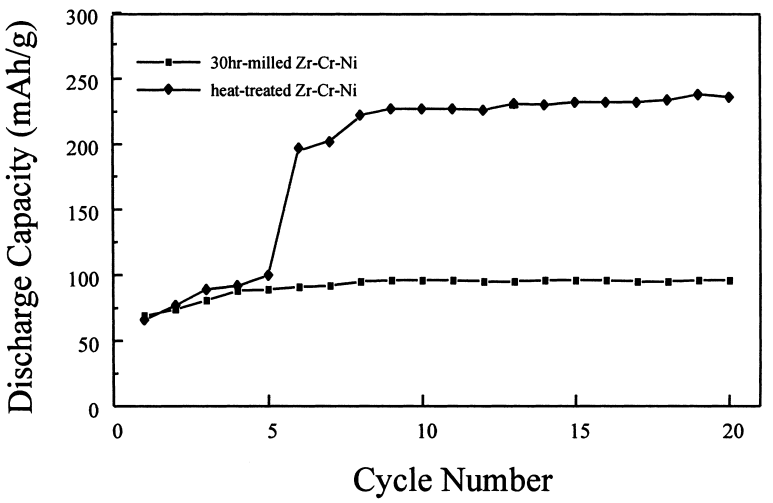

Fig. 6. Discharge capacity variation of 30 h-milled and heat-treated Zr–Cr–Ni electrodes with cycle number at room temperature.

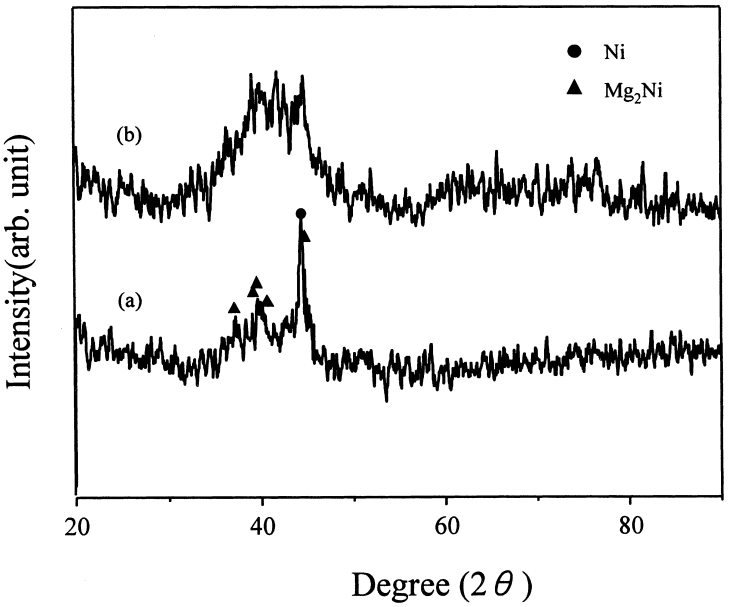

Fig. 7. X-ray diffraction patterns of 120 h-milled 2Mg–Ni and 1.8Mg–0.2Zr–Ni powders: (a) 120 h-milled 2Mg–Ni; (b) 120 h-milled 1.8Mg–0.2Zr–Ni.

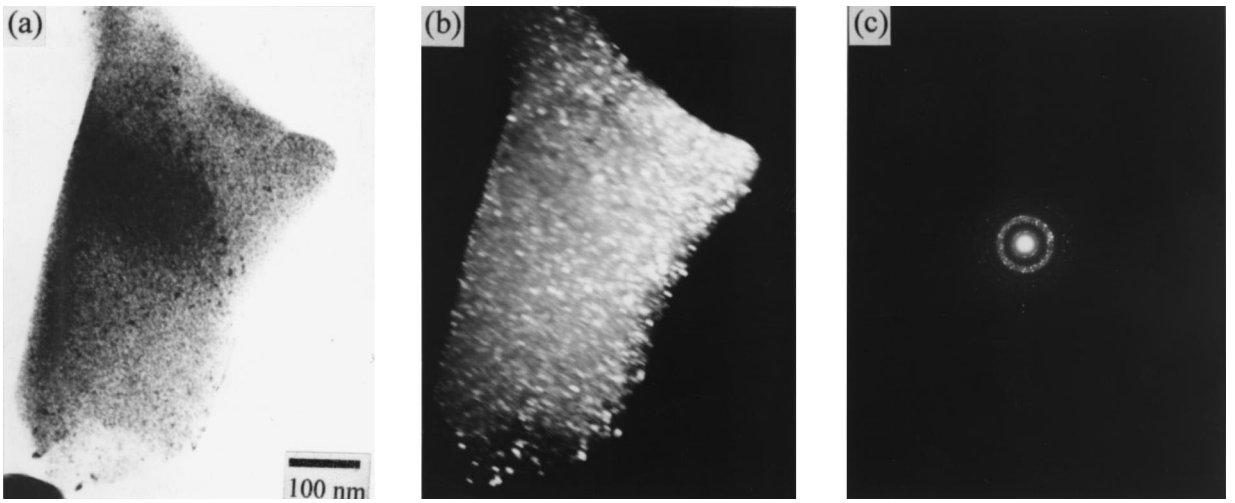

Fig. 8. TEM micrographs of the 120 h-milled 2Mg–Ni powders: (a) bright field; (b) dark field; (c) electron diffraction pattern.

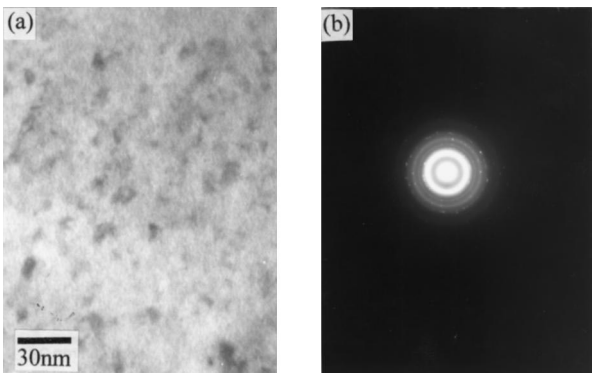

Fig. 9. TEM micrographs of the 120 h-milled 1.8Mg–0.2Zr–Ni powders: (a) bright field; (b) electron diffraction pattern.

line Mg_2Ni powders can absorb and desorb a large amount of hydrogen at lower temperature than 300°C and the required temperature for hydrogenation of nanostructured Mg_2Ni is lower than that of the conventional polycrystalline one. The absorption amount at 200°C is similar to the result of mechanically alloyed Mg_2Ni reported by Zaluski et al. [24], however, the desorption results have not been reported yet.

Fig. 10 also shows the hydrogen desorption characteristics at 30°C and 200°C for the 120 h-milled 1.8Mg–0.2Zr–Ni powders. The *P–C* isotherm at 30°C shows that 1.8Mg–0.2Zr–Ni powders absorbed 2.3 wt% of hydrogen which is three times larger than that of 120 h-milled 2Mg–Ni. At 200°C, hydrogen uptake equals about 3.0 wt% and the reversible amount of about 2.0 wt% hydrogen

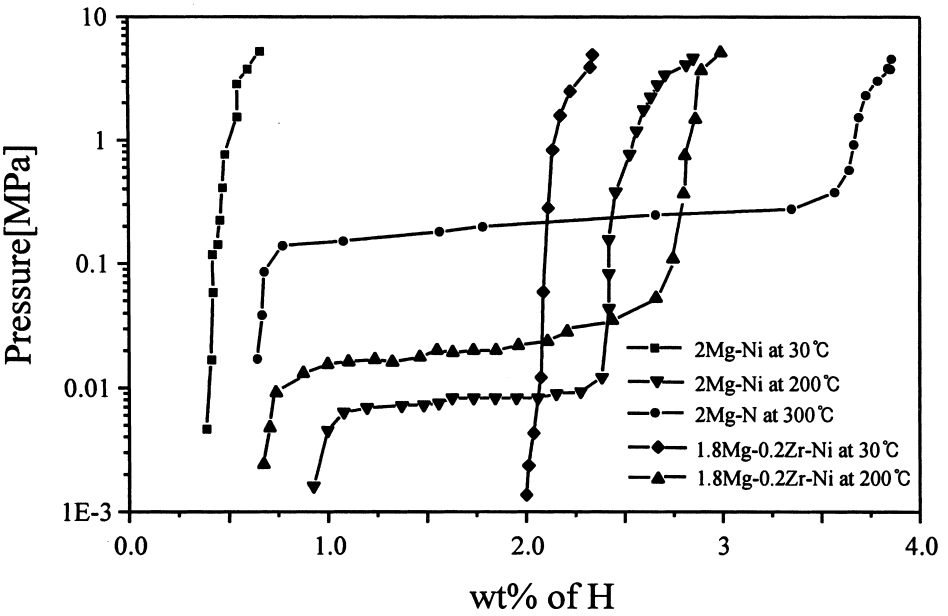

Fig. 10. Pressure–composition isotherms of 120 h-milled 2Mg–Ni and 1.8Mg–0.2Zr–Ni powders.

was desorbed at the plateau pressure of about $2.0 \cdot 10^{-2}$ MPa.. The amount of desorbed hydrogen at plateau pressure is increased by substitution of Zr for Mg and the plateau pressure was shifted to higher pressure at 200°C. The difference between 2Mg–Ni and 1.8Mg–0.2Zr–Ni in *P–C* isotherms seems to result from different microstructure and alloy composition. *P–C* isothermal results at 30°C and 200°C imply that hydrogenation characteristics at low temperature (below 300°C) can be improved by partial substitution of Zr for Mg.

3.2.3. Electrochemical measurements

Fig. 11 shows the variation of discharge capacity at 30°C with cycle number. The discharge capacity of 120 h-milled Mg_2Ni electrode was 170 mAh g^{-1}. It is much higher than that of the polycrystalline one which was reported by Iwakura et al. [4] and Cui et al. [25]. Iwakura et al. reported that the discharge capacity of the polycrystalline Mg_2Ni alloy electrode was very low (about 20 mAh g^{-1}) at 30°C but increased greatly at 70°C (maximum 400 mAh g^{-1}) and 90°C. Cui et al. reported that Mg_2Ni

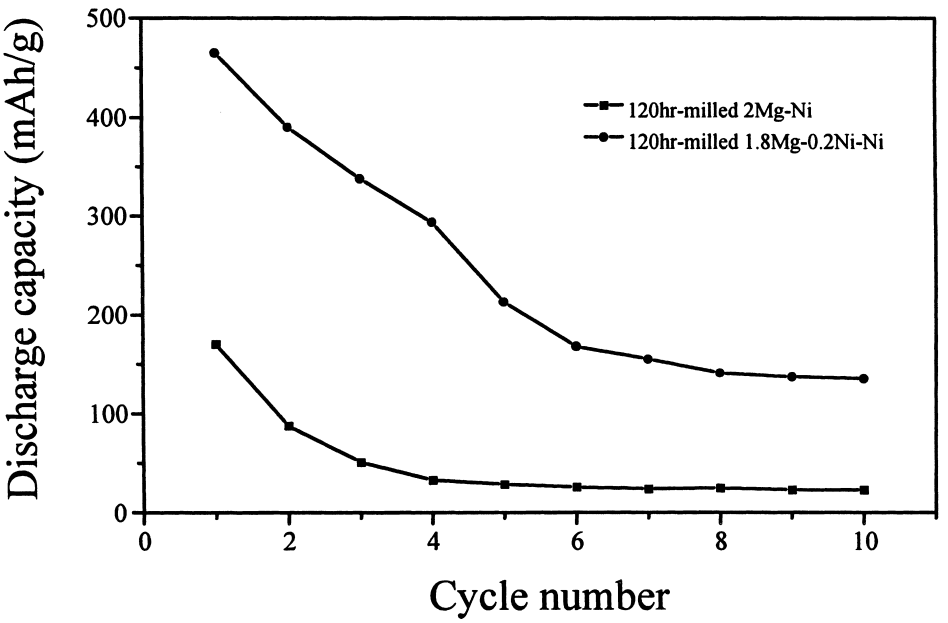

Fig. 11. Discharge capacity variation of 120 h-milled 2Mg–Ni and 1.8Mg–0.2Zr–Ni electrodes with cycle number at 30°C.

electrode prepared by the sintering method has very low discharge capacity (8 mAh g^{-1}). The formation of nanostructured alloys by mechanical alloying improved the electrochemical hydrogenation ability of Mg_2Ni electrode at low temperature and this result coincides with the result of *P–C* isotherms.

The discharge capacity of the electrode of 120 h-milled Mg_2Ni was maximum at the first cycle but decreased rapidly. Similar to the Zr–Cr–Ni system, the good activation characteristics of Mg_2Ni seems to be related to the small grain size and the defects introduced by mechanical deformation. The rapid degradation seems to result from corrosion of Mg in the alkaline KOH solution. Lui et al. [26] reported that the corrosion of Mg in the amorphous Mg–Ni alloy into $Mg(OH)_2$ in the alkaline KOH solution was the main cause for the capacity deterioration of amorphous Mg–Ni electrode. In contrast to electrochemical measurement, nanocrystalline Mg_2Ni alloy was not rapidly degraded in the *P–C* isothermal experiment. Therefore, the degradation of this alloy electrode seems to be due to the 6 M KOH alkaline solution. A further study is being performed for the degradation mechanism of nanocrystalline Mg_2Ni electrode.

Fig. 11 also shows the discharge capacity of substituted alloy electrode with cycle number. The partial substitution of Zr for Mg increased the discharge capacity of nanocrystalline Mg_2Ni electrode to 465 mAh g^{-1}. The increase of the discharge capacity at low temperature seems to be related with the greatly increased hydrogen absorption amount at 30°C and the increased amount of absorbed and desorbed hydrogen at 200°C.

4. Conclusions

The discharge capacities of the ball-milled electrodes was much lower than that of the as-melted one because $ZrCr_2$ type hydrogen storage alloy was not formed by 30 h ball milling. However, the ball-milled powder could be transformed into the C14 type Laves phase by heat-treatment with the microstructure of grain size smaller than 100 nm, and showed a similar discharge capacity as the as-melted $Zr(Cr_{0.5}Ni_{0.5})_2$. In addition, the activation behavior was improved owing to the smaller grain size and the defects from the mechanical deformation.

In contrast to the Zr–Cr–Ni system, nanostructured Mg_2Ni alloy was formed by 120 h-milling of elemental powders. Nanostructured Mg_2Ni powders absorbed and desorbed a large amount of hydrogen at 200°C, which means that the required temperature for hydrogenation of nanostructured Mg_2Ni is lower than that of conventional the polycrystalline one. Nanocrystalline Mg_2Ni electrode had a much higher discharge capacity than that of the polycrystalline one and a good activation characteristic at low temperature (30°C), but they were degraded rapidly with cycle. The partial substitution of Zr for Mg increased hydrogen absorption and desorption amounts at low temperature (30°C, 200°C) and greatly improved the discharge capacity of the nanostructured Mg_2Ni electrode at 30°C.

Acknowledgements

This study is supported by the academic research fund of Ministry of Education, Republic of Korea, in 1997. This work was supported by the research center for Hydrogen Energy, KAIST.

References

[1] J.J.G. Willems, Philips J. Res. 39 (1984) 1.
[2] J.J.G. Willems, K.H.J. Buschow, J. Less-Comm. Metals 129 (1987) 13.
[3] S. Wakao, H. Sawa, J. Furukawa, J. Less-Comm. Met. 172 (1991) 1219.
[4] J.J. Reilly, R.H. Wiswall Jr., Inorg. Chem. 7 (1968) 2254.
[5] J.C. Bolcich, A.A. Yawuy, H.L. Corso, H.A. Pertti, C.O. Anala, Int. Hydrogen Energy 19 (1994) 605.
[6] C. Iwakura, S. Hazui, H. Inoue, Electrochim. Acta 41 (1996) 471.
[7] J.S. Benjamin, T.E. Volin, Metall. Trans. 5A (1974) 1930.
[8] I.G. Wright, A. Wilcox, Metall. Trans. 1A (1976) 1203.
[9] J.S.C. Jang, C.C. Koch, J. Mater. Res. 7 (1992) 1519.
[10] E. Hellstern, L. Schultz, Phil. Mag. B 56 (1987) 443.
[11] E. Hellstern, L. Schultz, Mater. Sci. Eng. 93 (1987) 213.
[12] R.B. Schwarz, R.R. Petrich, C.K. Saw, J. Non-Cryst. Solid 76 (1985) 287.
[13] T. Mütschele, R. Kirchheim, Scr. Metall. 21 (1987) 135.
[14] T. Mütschele, R. Kirchheim, Scr. Metall. 21 (1987) 1101.
[15] R. Kirchheim, T. Mütschele, W. Kieninger, H. Gleiter, R. Birringer, T.D. Koblé, Mater. Sci. Eng. 99 (1988) 457.
[16] C.U. Maier, H. Kronmüller, J. Less-Comm. Met. 172–174 (1991) 671.
[17] A.K. Niessen, F.R. de Boer, R. Boom, P.F. de Chatel, C.W.M. Mattens, Miedema, CALPHAD 7 (1983) 51.
[18] T.B. Massalski, Binary Alloy Phase Diagrams, ASM, Metals Park, OH 44073.
[19] C.B. Jung, J.H. Kim, K.S. Lee, J. Alloys Comp. 267 (1998) 265.
[20] C.B. Jung, J.H. Kim, K.S. Lee, Nanostruct. Mater. 8 (1998) 1093.
[21] L. Zaluski, P. Tessier, D.H. Ryan, C.B. Doner, A. Zaluska, J.O. Ström-Olsen, L. Trudeau, R. Schulz, J. Mater. Res. 8 (1993) 3059.
[22] L. Zaluski, A. Zaluska, J.O. Ström-Olsen, J. Alloys Comp. 217 (1995) 295.
[23] A.K. Singh, A.K. Singh, O.N. Srivastava, J. Alloys Comp. 227 (1995) 63.
[24] L. Zaluski, A. Zaluska, J.O. Ström-Olsen, J. Alloys Comp. 217 (1996) 245.
[25] N. Cui, B. Luan, H.J. Zhao, H.K. Liu, S.X. Dou, J. Power Sources 55 (1996) 271.
[26] W.H. Liu, Y.Q. Lei, D.L. Sun, J. Wu, Q.D. Wang, J. Power Sources 58 (1996) 243.